MECHANICAL OXIDATION AND MICROPARTICLE PRODUCTION: A QUANTITATIVE STUDY OF MECHANICAL PLASTIC WEATHERING USING NOVEL REACTOR DESIGN

By

Claire Hartwig Alberg

A thesis submitted to the faculty of the University of Minnesota in partial fulfillment of the requirements for the degree of

MASTER OF SCIENCE

Boya Xiong
May 2022

Abstract

Mechanical degradation of plastic waste is a major source of microplastics and potentially a large contributor to the oxidation of plastic waste in soil and water environments. Mechanical oxidation of plastic occurs when mechanical force induces homolysis of covalent bonds on the carbon backbone and radical formation then leads to radical induced oxidation. Despite the abundance of mechanical degradation of plastic and its potential for oxidation in the natural environment, a quantitative understanding of this is the least pursued compared to other plastic oxidation mechanisms such as UV oxidation. This thesis attempts to generate a quantitative correlation between input of mechanical work and both oxidation of plastic and nano/microplastic production. In this device a low-density polyethylene sample sealed at the bottom of a glass cylinder is covered with sediment; the device is then fixed onto a shaker table, driving a circular motion of sediment. With a high-speed camera, sediment motion is captured and the calculated path length of the sediment in tandem with the coefficient of kinetic fiction between the sediment and the plastic substrate is used to calculate abrasive energy input. By employing X-ray photoelectron spectroscopy (XPS), quantification of the degree of oxidation due to a calculated abrasive energy input is made possible. In addition to the investigation of oxidation, a combination of total organic carbon measurements and nanoparticle tracking analysis is used to quantify the rate of nano and microplastic production and chemical leachate generation in a five-month weathering experiment. The novel findings from these experiments present an overlooked pathway, and the novel device generated will enable a high throughput testing platform for new materials and enable exploration that enhances our understanding of the effect of complex environmental conditions on plastic degradation.

Acknowledgements

I would like to thank all the members of the Xiong Lab for their support. In particular, I would like to thank Phoebe Keyes for her continued support and helping to introduce me to the world of research. I would also like to thank Ehsanur Rahman for all his work with the AFM to help establish the energy input model, as well as for taking over this device and making it even better. Finally, I would like to thank Boya Xiong for her efforts in training me as a researcher and scientist.

Contents

List of Figures and Figure Descriptions

List of Tables and Table Descriptions

1. INTRODUCTION

1.1 Environmental Impact of Plastic Pollution

Low Density Polyethylene (LDPE) is a pervasive contaminant in the environment because of its widespread commercial and industrial use. It has been used widely in many different industries for years due to its low production cost, light weight, and durability and because of this, polyethylene makes up 36% of all plastic waste (Geyer et al., 2017). In addition to bulk plastic contaminants, micro- and nano-sized plastic particles have also been discovered in all environmental compartments and are hypothesized to be degradation products from bulk plastic waste. This bulk plastic waste finds its way into the environment through rampant mismanagement of plastic waste and improper disposal (Geyer et al., 2017). To accurately estimate the timescales and pathways of plastic degradation in the environment, it is important to consider the natural processes that can increase the rate of degradation of plastic (Chamas et al., 2020). These natural processes include biofouling, chemical degradation, and mechanical degradation (Jahnke et al., 2017). To better understand environmental plastic degradation, these pathways have been simulated and studied in bench scale weathering experiments. Some weathering studies in the past have attempted to investigate the oxidation of plastic due to environmental conditions. Most weathering studies, however, have solely been focused on photo-oxidation (Giesse et al., 1988, Tribedi et al., 2017, Suresh et al., 2011). In contrast, oxidation by mechanical stress in the environment has not been thoroughly discussed in an environmentally relevant way. More importantly, previous work lacks the quantitative tools to examine the degree of oxidation that can occur by specific amounts of input energy to the plastic.

Mechanical oxidation is a neglected mechanism of oxidation to plastic in the natural environment, even though it is just as widespread as photo oxidation. In most environments where plastic waste ends up, especially in soil and in aquatic environments, there is an abundance of mechanical forces that could lead to mechanically induced chain scission and oxidation. Some specific environments that could be considered "hotspots" of mechanical degradation and oxidation of plastic are the sea swash zone (Chubarenko et al., 2020), the open ocean (Kalogerakis et al., 2017), and in agricultural fields (Wahl et al., 2021). Force is applied to plastics in marine environments from the motion of sand and water, for instance, the shear force of breaking waves in the open ocean or abrasion by the beach sediments in the swash zone. In agricultural practice, plastic is often intentionally used and left in fields as a cover to protect young plants and soil. When the field is plowed in the future, any remaining bulk plastic is subject to grinding and stress by sediments during plowing.

After bulk plastic in the environment has been oxidized and broken down mechanically into micro- and even nano- sized particles via shear force and sediment abrasion, it becomes more mobile and can spread faster in environmental systems than its bulk plastic counterparts. The chemical and physical fate of plastic in the natural environment has become a major concern as its degradation byproducts could have unknown impacts on human and environmental health. One major concern is that plastic has been known to sorb hydrophobic contaminants that are known to be harmful to the health of different animals as well as humans. Contaminants that are known to sorb onto plastic surface are antibiotics, polychlorinated biphenyls (PCBs), and polyfluoroalkyl substances (PFAS) (Smith et al., 2018). These contaminants with known human health

effects sorb to the micro/nano-plastic surface and can then be ingested and bioaccumulate in the bodies of humans and animals. Furthermore, oxidation of plastic increases the number of oxygen containing functional groups on the surface of the polymer in addition to increasing its surface area, both of which facilitate increased adsorption of the dangerous contaminants to the plastic surface (Lan et al., 2021).

There have also been studies on the toxicity of nano-plastics themselves. There was one study in which heightened concentrations of nano-plastics in the fish embryos caused increased cell death. Perhaps an even more alarming finding in this study was that at the nano scale plastics can even enter bodies passively through pores in the skin rather than being actively ingested (Enfrin et al., 2020). There has also been a study which found nano-plastics had toxicological effects on the epithelial cells in human lungs (Xu et al., 2019). Preliminary studies have also found that there is a correlation between increased microplastic concentrations in drinking water and irritable bowel disease (Yan et al., 2021). Oxidation accelerates production of these extremely mobile micro and nano-particles because it embrittles the plastic which makes it easier to break down (Hsu et al., 2012). These alarming findings all imply an urgent need for investigation of how such particles are being produced in the environment and the pathways in which humans can be exposed to them.

Studying mechanical oxidation in a fundamental and quantitative way is imperative in understanding this less explored degradation pathway. It will play an important role in assessing the risk that existing plastic pollution poses to human health and the environment. Quantitative investigation of common degradation mechanisms, such as oxidation, will also likely play a key role in future sustainable polymer development

1.2 Mechanical Oxidation

To quantitatively study mechanical oxidation, it is important to understand the fundamental process through which it occurs. Early research on mechanical oxidation attempted to deconvolute the complicated process and investigate it. Mechanical oxidation is mechanochemical, and thus it is difficult to deduce which aspects of it stem from mechanical force. The oxidation process itself is undoubtedly a chemical process, but the mechanism that initiates it is more ambiguous. In previous experiments, it was made clear that mechanical input was inducing chain scission and generating radicals on the plastic surface. However, it was unclear whether the mechanical force itself was causing chain scission, or the chain scission was caused by the local increase in heat from friction on the surface of the polymer. After a series of experiments at liquid nitrogen temperatures where the thermal effects were eliminated, it was confirmed that mechanical force alone was sufficient to generate chain scission and form radicals (Sohma, 1989).

One of the first applications where mechanical oxidation of polyethylene was observed was in human joint implants made of ultrahigh molecular weight polyethylene. Joint implants could also be considered a degradation hotspot because abrasive wear in joint implants is inevitable. The reason that mechanical oxidation was first observed in joints was due to the fact that implants reside in human bodies for prolonged periods of time and therefore, their degradation demands close monitoring. Initially the majority of oxidation was thought to be caused by the sterilization process of the joint, but after the sterilization process was amended to decrease preliminary oxidation, oxidation *in vivo* was still observed (Kurtz et al., 2005).

The hypothesized reaction pathway of oxidation is supported by the findings in preliminary experiments where UHMWPE (ultra-high molecular weight polyethylene) was subjected to mechanical force and then underwent careful surface characterization with Fourier transform infrared spectroscopy (FTIR) and electron spin resonance spectroscopy (ESR) (Fanconi et al., 1982). This pathway is illustrated below in **Figure 1.1**. The reaction is initiated by homolytic chain scission of the carbon-carbon backbone of the polymer, induced by mechanical force. Radicals are generated from this chain scission event and can then form a vinyl end group through end chain β scission, a methyl end group through disproportionation, or a carbonyl group in the presence of oxygen.

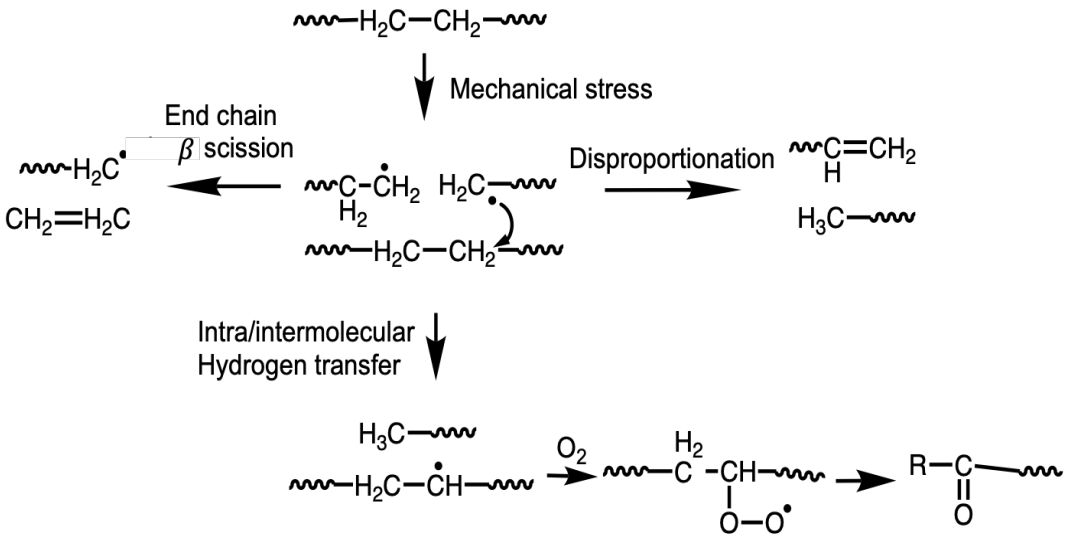

Figure 1.1. The mechanical oxidation chemical pathway that has three different end points: either a vinyl end group, a methyl end group, or, a carbonyl group when oxygen is present in the system.

Given that mechanical oxidation is both a physical and chemical process, there are many things that could potentially influence the rate at which it occurs. Mechanical oxidation is initiated by mechanical chain scission, so the rate of chain scission in a system

will dictate the rate of mechanical oxidation. More intense forces are likely to generate more instances of chain scission in the system. This implies that heavier and sharper sediments would likely generate more oxidation due to the increase in the abrasive wear rate from the more angular abrasive particles (Stachowiak, 2001) and the increase in normal load from the heavier particles. The fact that the process being investigated is oxidative also means that the abundance of oxygen in the media surrounding the plastic (air or water) will influence the amount of oxidation happening on the surface of the plastic as well. In addition to the size and surface asperities of abrasives, it was found, in microtoming experiments, that the presence of transition metals in the microtome blade also increased the rate of oxidation (Jacobson et al., 2001). This implies that the composition of the abrasive material in the system would also influence the rate of oxidation on the plastic surface. Finally, because mechanical oxidation involves an oxidative chemical reaction, it is hypothesized than an increase in temperature will increase reaction rate and thus increase the rate of oxidation.

1.3 Previous Work and Knowledge Gaps

To truly understand mechanical oxidation in the environment, a quantitative correlation between environmentally relevant force conditions and the level of oxidation they generate is needed. To create such a correlation, both oxidation and force input need to be quantified in the experimental design. Previous studies on mechanical degradation of polyethylene lack quantification in their method. There have been multiple studies that replicate environmental conditions at a bench scale such as a sea swash zone using a concrete mixer (Chubarenko et al., 2019, Efimova et al., 2018) and fluid shear in high turbulence environments using mechanical impellers (Enfrin et al., 2020, Ekvall et al.

2022). In summary, careful analysis and characterization on microparticles exists in previous studies, but they lack quantification and justification of the input energy in degrading plastics. In studies on the mechanical oxidation of polyethylene, microtoming was used (Jacobson et al., 2001) and grinding of polyethylene at liquid nitrogen temperatures (Fanconi et al., 1982). While these studies both featured very careful quantification of oxidation on the plastic after weathering using FTIR, ESR, and chemiluminescence, the weathering of the plastic was not environmentally relevant.

To properly investigate the fundamental mechanism of mechanical oxidation and assess its contribution to plastic degradation, both the force input in the system and the resulting oxidation need to be carefully quantified. This experimental setup aims to quantify the input energy of well characterized sediment motion and the resulting oxidation through sensitive surface characterization (x-ray photoelectron spectroscopy) to fulfil both of those requirements. The data of both work (input energy) and the resulting oxidation will then be used to create a quantitative correlation between the two.

1.4 Objectives and Hypothesis

The testable hypothesis that will be investigated within this thesis is that mechanical abrasive wear of plastics occurs in environmental conditions such as in aquatic and soil environments and then causes chain scission and mechanical oxidation. Furthermore, the mechanical work in the system can then be correlated with an increase in oxidation, microparticle production, and adsorption.

From combining the theoretical knowledge gaps established during literature review with the goals established in the experimental plan, there was a list of objectives that were developed. Given the large range of conditions and corresponding method blanks

that needed to be studied to fulfil such goals, the first objective was to develop and test a novel high-throughput reactor to study mechanical degradation. After the reactor had been constructed and tested, the second objective was to investigate the degree of mechanical oxidation of plastic in a simulated aquatic environment. The final objective was to correlate the quantity of work done on the plastic surface with nano/microplastic generation from mechanical degradation of low-density polyethylene (LDPE).

2. MATERIALS AND METHODS

2.1 Reactor Design and Construction

After deciding what was going to be investigated by review of mechanical oxidation and mechanical degradation in the natural environment, a list of requirements for the desired features in device design was established. It was important that this list of design requirements in tandem could achieve a quantitative correlation between input energy, oxidation, and microparticle production unlike methods specified in previous work. It was also important that the knowledge gaps identified would be investigated in an environmentally relevant manner.

The first design requirement was that the fluid in the system needed to be recirculated rather than collected in an effluent because the concentration of nanoparticles would be far too low for analytical techniques. It was hypothesized, under the low load of sediment abrading plastic in the experimental design, that the rate of nano-plastic generation from bulk plastic would be slow, so the concentration of nano-plastics generated was expected to be low. To ensure a measurable nano-plastic concentration in a reasonable timeframe that could then be correlated to input energy, it was imperative that the nano-

plastics generated during weathering were retained in a batch reactor system. In addition to a batch reactor system, the fluid needed to be moved without pumps or paddles, because a pump or an impeller would introduce an external force to the generated nano/microplastics that is difficult to quantify. This would make quantification of input energy in the system nearly impossible. Furthermore, to design an environmentally relevant system, the effect of temperature needed to be considered, thus temperature control was also a requirement. Finally, to ensure that there was no microparticle contribution from the device itself, it was imperative that any portion of the device that was in contact with the fluid sample was not made of plastic.

Another theory that guided reactor design, and that would enhance the novelty of this mechanical weathering experiment, was that the work done on the surface of the plastic needed to be characterized. It also needed to emulate a specific environmentally relevant mechanical weathering mechanism. This was done by combining easily characterized sediment motion with fundamental physics equations to generate a rudimentary model for the work done on the surface of LDPE film by a single sliding piece of sediment:

$$Work = \mu \times F_N \times S \quad (1)$$

Where μ is the coefficient of kinetic friction between the sediment and the plastic surface (with the water interface), F_N is the normal force of a single piece of sediment, and S is the path length of the sediment traveling along the surface of the plastic

Having plastic serve as the substrate changes the environmental focus slightly from the majority of experiments with free floating plastic. Free floating plastic being acted upon by fluid shear or sediment abrasion is much more representative of the plastic pollutants

that are suspended in the open ocean. This design is much more similar to sediment embedded in beach sediments in the sea swash zone (Chubarenko et al., 2020), buried in lake sediments, or plastic residing in a soil environment (Wahl et al., 2021), where a fluid component could be periodically encountered during rainstorm or field watering events.

After deciding on which parameters and blanks needed to be considered for the experiment it was concluded that the device also needed to have a high throughput to accommodate the many samples that needed to be weathered. A high throughput design was also important because many materials testing methods are trending towards high throughput reactors as they are efficient and effective at testing many different materials, and in some cases conditions, simultaneously (Potyrailo et al., 2011). To make the reactor design feasible as well as easily reproducible, common lab equipment was used as the base for the design. The result of the reactor design process was a well plate design that was watertight to contain the fluid portion of the sample.

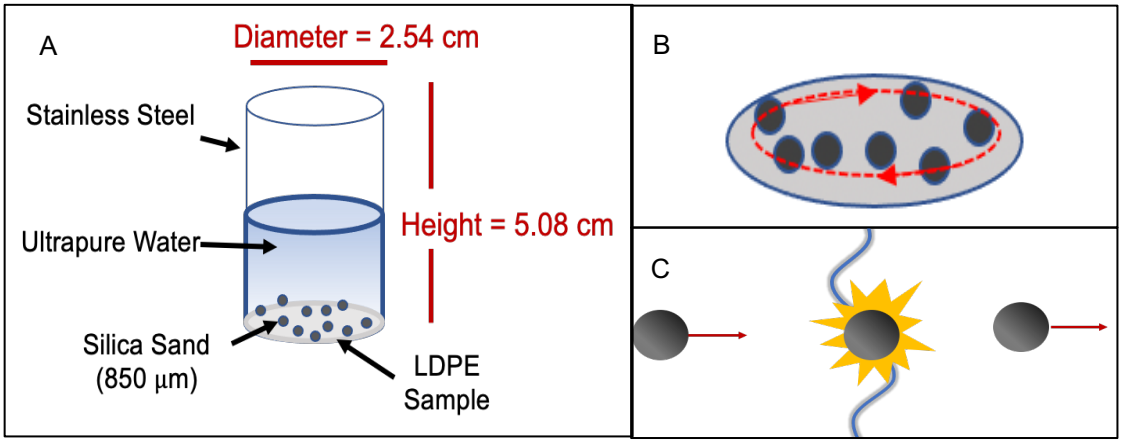

Figure 2.1 Flow cell reactor design. (A) Each stainless well has an outer diameter of 2.54 cm, and a height of 5.08 cm with a thickness of 0.127 cm. 4 mL of water and 400 mg of sediment a size of 850 µm was added above plastic substrate. (B) Intended sediment motion by the reactor design. (C) Conceptual depiction of the sediment causing polymer chain scission and inducing mechanical oxidation.

The design features 5 main components that were securely mounted to the top of a shaker table. A shaker table was chosen as the moving component of this design because it is commonly found in lab settings which makes the design very replicable. From the bottom up, the first component is an intermediate Delrin plate (McMaster-Carr 8575K145) that was threaded in a grid fashion so that the well holders could be securely mounted to the shaker table. The grid of the holes used for mounting was designed to maximize the capacity of sample holders that could be mounted. Delrin was chosen because it is relatively light and it has good structural integrity. Initially these plates were constructed of stainless steel which was too heavy and caused the shaker table to become imbalanced during shaking. To facilitate triplicate samples, three wells were mounted together into one well holder. It was then easy to remove three samples without disturbing other samples that required longer weathering times. The bottom component of the fluid cell (piece 1 in **Figure 2.2 (A)**) was made of Delrin (McMaster-Carr 8575K145) and had three holes to house wells. Within the three holes there were O-rings (piece 2 in **Figure 2.2 (A)**) that were placed in a groove within the hole walls. With the addition of the O-ring the slightly smaller diameter well would sit inside the O-ring and create a watertight seal. The wells themselves (piece 3 in **Figure 2.2 (A)**) were made of stainless-steel tubing with an outer diameter of 1 inch and a length of 2 inches (McMaster-Carr 8989K838). This was utilized because it was an accessible standard sized tubing that could easily be cut to the desired lengths. For future experiments, the wells will be replaced with custom made glass wells (manufactured by Quark Glass, LLC) for reasons that will be explained in the results section. The next piece up from the bottom of the reactor (piece 7 in **Figure 2.2 (A))** was also made of Delrin and was used to clamp the design together and help the seal. This piece

was connected to the second piece through a standoff (piece 6 in **Figure 2.2 (A))** and a screw that connected the top and bottom pieces of Delrin and helped it apply pressure to the well piece when properly tightened. The fifth and final piece was made from clear acrylic (piece 8 in **Figure 2.2 (A))** (McMaster-Carr 8560K358) and was used to make sure sand motion could be imaged through the lid of the reactor. This also facilitated the observation of water levels in each well throughout the run of the experiment. The detachable sample holder module can be removed by unscrewing and ensured that the sample can be removed from the setup without destroying or abrading the surface, this also makes the design easy to modify for different experimental needs.

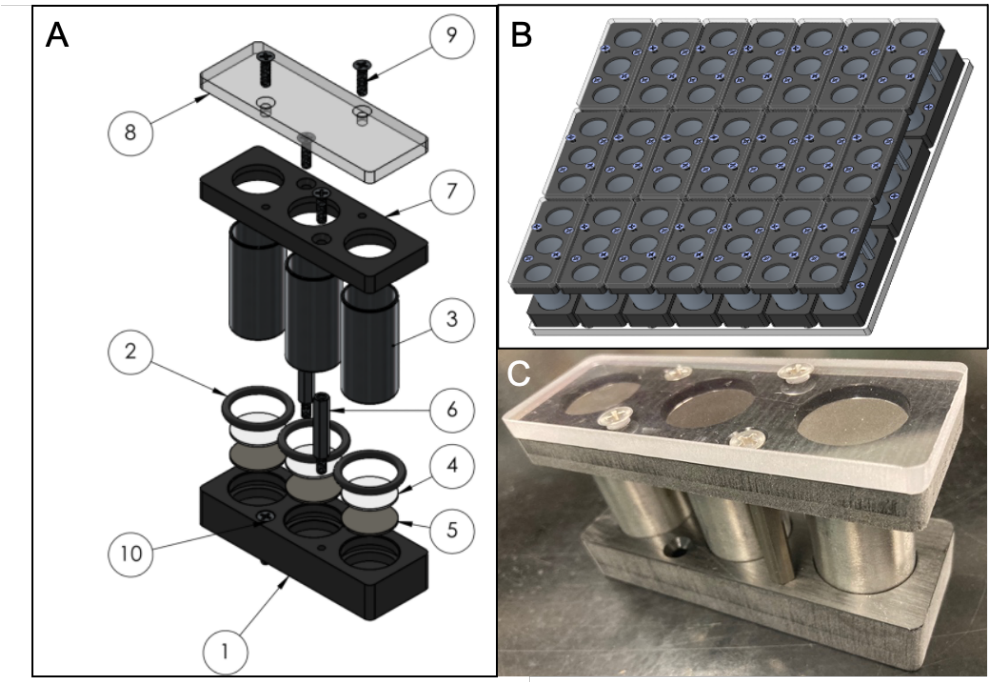

Figure 2.2 Flow cell reactor assembly. (A) an exploded diagram of the assembly with 1) the bottom piece of Delrin 2) the O-ring used to generate a water tight seal 3) the stainless steel well 4) the LDPE sample 5) a PEEK disk to ensure no reaction between the Delrin and the LDPE at higher temperatures 6) the standoff used for the clamping mechanism 7) the top piece of Delrin also used in the clamping mechanism 8) the piece of acrylic used the seal the reactor 9) the screw to affix the acrylic lid and 10) the screw to affix the whole sample holder the intermediate Delrin plate (B) how the setup sits on a shaker table (C) An image of the final product after it had been manufactured by the University of Minnesota College of Science and Engineering Machine Shop.

2.2 LDPE Sheet Preparation

To ensure the virgin samples do not have any weathering or contamination from storage and handling, and the surface of the virgin samples was as smooth and clean as it could be, the samples were hot-pressed from commercial pellets. A Genesis Hydraulic Compression Press from Wabash was used to press the plastic sheets. Between 5 and 6 grams of LDPE pellets (DOWLEXTM 2045G) were placed in a small approximately circular monolayer on a sheet of mirror coated stainless steel on the lower platen of the press. After this a sheet of Kapton film was then placed on top of the pile of pellets. The mirror coated stainless steel and the Kapton film were used to ensure a smooth surface of

the virgin plastic. The platens of the press were heated to 180ºC and brought together at a pressure of 9.81×10^5 N for 1 minute, 1.96×10^6 N for 1 minute, and 3.92×10^6 N for 1 minute. The mirror coated steel, pressed pellets, and Kapton were then removed from the press and immediately cooled with cold iron blocks. This procedure resulted in a sheet with a thickness of approximately 0.5 mm. The Kapton film was then carefully peeled off from the surface of the freshly pressed LDPE sheet and the sample was pried off the mirror coated steel. The pressed sheet was gently placed between two clean pieces of printer paper and stored in a vacuum chamber to limit further oxidation from the surrounding atmosphere until cutting.

The freshly pressed plastic sheets were then carefully cut into circles with a 2.54 cm diameter punch and heavy hammer. The punch was cleaned using acetone and allowed to dry completely to ensure that the surface of the virgin plastic was not contaminated by any organic residue on the blade of the punch. The plastic was placed on a clean metal sheet to provide a sufficiently hard surface for the punch to cut through the LDPE sheet. The punch was placed carefully on the surface of the plastic and then hit with a heavy hammer approximately 5 times. The 2.54 cm plastic circle generated was then carefully removed from the punch and rinsed with ultrapure water to remove any debris that could have accumulated on the surface during cutting. The cut sheets were then stored in a vacuum chamber until use.

2.3 Mechanical Weathering Experiments

The cut LDPE circles were mounted into the sample holders with care to avoid scratching. Prior to installation, samples weight, the weight of the sediment, and the sample thickness were all recorded. Each well was marked with a number corresponding to a data

entry table. The conditions in which the sample would be weathered (room temperature or 50ºC) were also recorded in this table. The sediment in the setup that was used was ASTM grade 850 µm silica (Humboldt H-3820) that was acid washed with 0.5 M HCl before use. The acid washing was done by submerging the silica in HCl in a glass solvent bottle and sonicating for 10 minutes, then the silica was left to soak in the bottle overnight and sonicated again for 10 minutes the next day. After the silica was removed from the HCl it was then rinsed 5 times with ultrapure water and left in an open solvent bottle in the hood to dry. After data entry for the sample was completed, the sample and the silica were placed carefully into the bottom of the sample holder on top of a small disk of PEEK plastic to ensure that no reaction occurred between the LDPE sample and the sample holder itself. The cell was then assembled, and 4 mL of ultrapure water was pipetted into each of the wells using a glass pipette to limit possible cross contamination of microplastics in the fluid sample. The acrylic plate was the last piece to be mounted for sample cell installation.

The sample holders were then secured to the top of their respective shaker tables and set to shake at 250 rotations per minute. The high temperature samples were set to weather at 50 ºC for the duration of their weathering. There was a significant amount of evaporation that occurred in both setups. The 50 ºC setup was refilled approximately twice a week and the room temperature setup was refilled approximately once or twice a month. To do so, the lid of each sample holder was first removed and approximately 3-4 mL of ultrapure water was put into the wells using a glass pipette. At the end of each weathering period the selected sample holders from each of the setups were removed. The fluid from each of the wells was then pipetted out using a new glass Pasteur pipette for each sample. The fluid sample was then transferred into a 25 mL amber bottle and the weight of the fluid

was recorded to determine the volume of the fluid sample. Ultrapure water was used in an attempt to rinse off residue on the sides of the well and added to the fluid sample that was taken directly from the well itself. The fluid was then stored in the refrigerator at 4ºC until analysis.

After the fluid was removed the cell was disassembled and a small amount of the silica from each sample was removed and then moved into a labeled well plate. The remaining silica was then disposed of and the plastic sample at the bottom of the well was then carefully removed using a clean pair of tweezers. Any touching of the sample was focused on the edge where analysis would not be performed. The plastic samples were then placed into a labeled well plate and placed directly into a vacuum desiccator to dry them for approximately seven days before XPS analysis (as XPS is very sensitive to any moisture).

The speed of rotation, amount of silica, and amount of water chosen to place in each well was chosen by preliminary experiments done with standard commercially available well plates with similar diameters of the wells in the final experimental design. The amount of silica sand that was chosen was determined, through trial and error, to coat the surface of the sample with an approximate monolayer of sand to try and eliminate silica particles resting on top of one another in the reactor and complicating the desired particle motion. The amount of water was optimized, again through trial and error, so that the cavitation of the water as it rotated did not reach all the way down to the sample surface and inhibit sediment motion. The speed which was chosen for the weathering was optimized utilizing slow motion video on an iPhone SE. In the video taken of the 250 rpm run (the speed which was chosen for the experimental design) the sediments were seen to

be moving across the sample surface, but were not becoming suspended, which was the desired motion for energy input quantification.

2.4 Sediment Motion Characterization

Sediment motion characterization was done through a rudimentary setup using a high-speed camera (Chronos 1.4 High Speed Camera). A shaker table was suspended upside down, and a glass scintillation vial with approximately the same dimensions as the wells in the experimental design was adhered to the shaker table using carpet tape. Prior to the attachment, the scintillation vial was filled with ~ 400 mg of sediment and 4 mL of water and the shaker table was set to rotate at 250 rpm which corresponds to a linear speed of about 1.99 m/s, to match experimental conditions. The shaker table speed was obtained by making a measurement of the shaker's radius of displacement from center and using that distance to calculate the circular path that the shaker table traveled. Then, using that path length and the speed in rotations per minute, the linear speed was obtained. The scintillation vial was also backlit to ensure that the imaging could have sufficient contrast. The high-speed camera was situated right under the glass vial and was set to take about 1 minute of video at one thousand frames per second. An open-source tracking software was used to calculate the average speed of the sediments in the setup.

2.5 Coefficient of Kinetic Friction Characterization

The coefficient of kinetic friction in the system was determined using atomic force microscopy (AFM) (Asylum research, MFP 3D). A 1μm rounded silica tip was used to

imitate the interaction between a piece of sediment in the system and the plastic substrate. The test was performed in water to make it more representative of the experimental conditions. The theory behind this experiment is to use Amonton's Law of friction:

$$\mu = \frac{F_F}{F_N} \quad (2)$$

Where μ is the coefficient of kinetic friction F_F is the frictional force is obtained from a lateral signal from a force transducer in the system and the normal load (F_N) is measured from the deflection of the AFM cantilever. In the experiment the normal load is linearly varied and, in response to that, the frictional force varies. The normal load values and frictional force values are then plotted and the slope of that line is determined to be the coefficient of kinetic friction. Amonton's Law has been extensively investigated for its application in experiments such as this and it has been found through experiments using AFM (nanoscale), Triboindentation (microscale), and SFA (macroscale) that the coefficient of kinetic friction has been found to be almost constant across 6 orders of magnitude on the length scale (the length being the radii of the indentation tip) (Gao et al., 2004). Given that the data in this experiment is only being extrapolated from 1 μm to 850 μm it can be assumed that the coefficient of friction obtained from the AFM experiment is representative of what is occurring in the system itself.

2.6 Nano-plastic characterization

To remove the non-plastic particles generated from the stainless-steel wells or silica, the sample was then centrifuged using the Thermo Fisher Sorvall Legend X1R for 30 minutes at 5,000 rpm to ensure that any silica/metal was settled out, it was determined that particles with a density similar to or higher than silica with a size of 30 nm would be

spun down to the bottom of the centrifuge tube. Note that this centrifugation would also remove any potential microbial contamination during storage. The supernatant was taken and kept at 4 °C for subsequent analyses. As polypropylene plastic centrifuge tube was used, proper control of just MQ water in plastic tube was also taken for TOC and particle analysis.

The nanoparticles in each sample were analyzed with nanoparticle tracking analysis (NTA) using a NanoSight LM-10 in the University of Minnesota Nano Center. After centrifugation, one of the triplicate samples from each well was sonicated for 10 minutes in the Nanomaterials lab immediately prior to measurement to eliminate any weak aggregation that occurred during centrifugation and storage. Roughly 0.5 mL of sample was utilized and a 30 second video was taken 10 times for different pockets of liquid in the sample. Samples that were too concentrated (>100 particles per frame) were diluted until an appropriate amount of separation between particles could be achieved.

As a proxy measurement, TOC was also completed using a Shimanzu TOC-L. Due to the minimum volume requirements for the TOC measurements, one mL of sample was diluted to 15 mL for the experiment. A new calibration curve was created every month for the measurements using a potassium hydrogen phthalate solution of 100 mg C/L. Samples were placed into 20 mL glass test tubes for the measurement and covered with parafilm to mitigate any evaporation or contamination from the atmosphere.

2.7 Plastic surface characterization

To analyze oxidation on the surface of the plastic samples x-ray photoelectron spectroscopy was performed using the PHI Versaprobe 5000 Scanning X-ray

Photoelectron Spectrometer. Samples for XPS were prepared by drying completely in a vacuum desiccator and cut to size using a sharp razor that had been cleaned with acetone. The sample was handled carefully using a pair of tweezers as even powderless gloves can leave a residue detectable by XPS. After sample preparation the sample was mounted to the sample holder using double sided tape. Survey measurements were conducted with a pass energy of 280 eV and an x-ray setting of 200u50W15KV. The high-resolution measurements to look at the spectra of specific elements (oxygen, silicon, and carbon) were conducted at a pass energy of 55 eV and an x-ray setting of 100u25W15KV.

3. RESULTS AND DISCUSSION

3.1 Input Energy Quantification

3.1.1 Sediment Velocity Results

Velocity of particles was calculated using the particle tracking system developed by Nicholas Ouellette. The system consists of multiple MATLAB scripts that identify particle in frames, consolidate tracks of moving particles, and calculate the particle velocity in pixels per frame as a surrogate for meters per second that can then be converted. The calculation was based on a total number of 7190 images. Parameters used for the program were a minimum contrast of 8 gray levels brighter than the background, minimum particle area of 100 square pixels, and maximum deviation from predicted position of 8 pixels. The program identified an average of 8.5 particles in each frame and 12,373 tracks of particle movement. Based on 27.3 pixels/mm and a video frame rate of 1000 frames per second, the average particle velocity was calculated to be 0.233 ± 0.056 m/s. This is within the environmentally relevant range of sediment transport velocities that exist between

suspended sediments and stationary bedload which is 0.063 m/s to 0.24 m/s (Yang et al., 2019).

3.1.2 Friction Coefficient Results

After performing scratch tests with the atomic force microscope using the methods described above in the methods section, the coefficient of kinetic friction for sediment abrasion in water was determined to be 0.299 ± 0.04.

3.1.3 Calculation of Input Energy

After obtaining the coefficient of kinetic friction between the sediment and the plastic substrate and the average velocity of a piece of sediment within the experimental setup it was possible to then calculate the different input energies for each time point. The force of friction was obtained by multiplying the normal load applied by a piece of sediment in the reactor by the coefficient of kinetic friction. The normal load was calculated using the equation below:

$$F_N = g \times [(\rho_s - \rho_w) \times V_s] \quad (3)$$

Where F_N is the normal load of a single piece of sediment calculated to be 8.4×10^{-6} N by multiplying the average sand particle volume by the specific gravity of the silica used, ρ_s and ρ_w are the densities of silica and water, respectively, V_s is the volume of a single piece of sediment, and g is the acceleration due to gravity near the earth's surface (9.81 m/s^2). These calculations were made assuming all pieces of sediment had a diameter of 850 µm and were perfectly spherical in shape. This equation incorporates both the gravitational and buoyancy forces acting on the sediment to provide a net normal load applied to the sediment surface. To obtain the force of friction (F_F) between the sediment and the plastic surface, F_N was then multiplied by the coefficient of kinetic friction. To obtain the input

energy from a single path of sediment around the plastic surface over the weathering time the equation below was utilized:

$$E = F_F \times v_s \times t \quad (4)$$

Where E is the input energy from a single piece of sand, v_s is the 0.233 m/s obtained from sediment motion tracking analysis, and t is the weathering time in seconds.

The total input energy is then calculated by determining the approximate number of pieces of sediment in each well and multiplying E by that number. The number of pieces of sediment in each well was calculated using the equation below:

$$N = m_T \div (\rho_s \times V_s) \quad (5)$$

Where N is the number of pieces of sediment in the well and m_T is the total mass of sediment in the well, which was recorded before placing it into the well. Input energies from both the 50 ºC and Room Temperature experimental setups were calculated from this set of equations and can be seen in **Table 3.1.**

Table 3.1. The calculated input energy from the sediment on the sample surface for both the room temperature and 50 ºC setups for the three time points at which the XPS data was taken. This reveals that even with blunt sand and a light force load, over long weathering time, a substantial amount of energy can be applied to the material surface within this experimental design.

sample	time (s)	path length (m)	number of pieces of sediment	input energy (J)
1 month Room Temperature	2.6×10^6	$6.0 \times 10^5 \pm 1.4 \times 10^5$	468	424 ± 191
1 month 50 ºC	2.6×10^6	$6.0 \times 10^5 \pm 1.4 \times 10^5$	469	425 ± 190
2 month Room Temperature	5.3×10^6	$1.2 \times 10^6 \pm 3.0 \times 10^5$	471	872 ± 390
2 month 50 ºC	5.3×10^6	$1.2 \times 10^6 \pm 3.0 \times 10^5$	470	872 ± 390
3 month Room Temperature	7.9×10^6	$1.8 \times 10^6 \pm 4.4 \times 10^5$	466	1288 ± 576
3 month 50 ºC	7.9×10^6	$1.8 \times 10^6 \pm 4.4 \times 10^5$	468	1293 ± 578

3.2 Plastic Surface Characterization

To investigate the degree of oxidation on the surface of the plastic, X-ray Photoelectron Spectroscopy (XPS) was performed. This was selected over other surface measurements such as Fourier Transform Infrared Spectroscopy (FTIR) as it detects the elemental composition of the sample surface with only a few nm of penetration depth. Characterizing plastic oxidation required a true surface measurement because it was hypothesized that the sediment abrasion under the low loads (~μN) in this experiment would only affect a shallow layer on the top of the sample surface. Note that the peak

intensity of XPS does not necessarily reflect the relative abundance of the element on different sample's surface. The peak intensity is a function of material, as well as the angle at which the x-ray beam hits the sample surface. Given that the plastic samples all had varying amounts of metal deposit on them, and each sample had to be mounted and placed into the chamber separately so that the angle between different samples could have changed slightly, the peak intensities would most likely not be consistent from sample to sample. (Brundle et al., 2020).

3.2.1 Virgin LDPE Characterization

Using XPS, the pristine LDPE surface was found to contain 8.12% oxygen (**Table 3.1.**) and the location of the oxygen peak (~532 eV) in high-resolution oxygen XPS data corresponds to the carbonyl group (Russo et al., 1998). This peak can be seen in the virgin sample in **Figure 3.3**. The existence of carbonyl functional groups on the surface of the virgin plastic was corroborated by the high-resolution carbon XPS data as a small peak at ~289 eV is present (**Figure 3.2)** which is indicative of carbonyl formation (Briggs et al., 1992). It is hypothesized that this oxygen on the virgin sample was most likely thermal oxidation from the pressing process and potentially some sort of organic contaminant on the surface of the plastic. Furthermore, Ca deposit was detected which is a common environmental contaminant from dust ($CaCO_3$) and could contribute to oxygen percentage.

3.2.1 Preliminary XPS Data

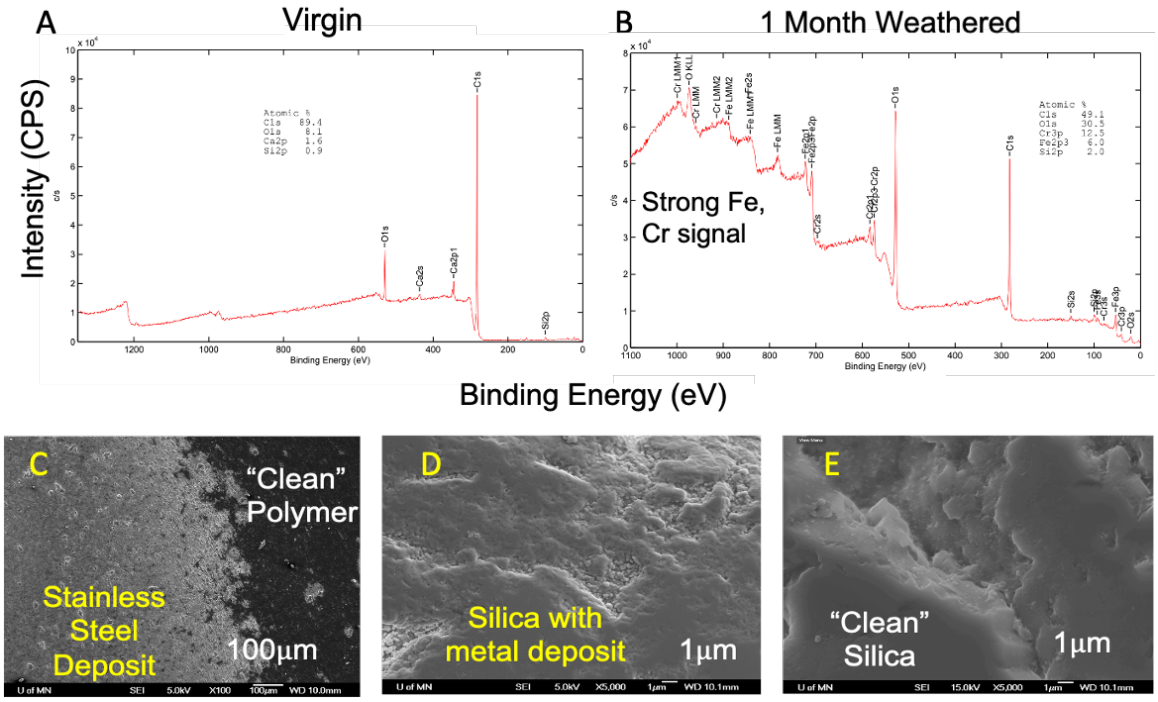

Figure 3.1. Preliminary XPS and SEM results of the sample surface (A) an XPS survey spectrum of the virgin plastic (B) an XPS survey spectrum of the one month weathered plastic revealing chromium and iron signals (C) SEM image of the delineation between the deposit and a cleaner part of the polymer (D) SEM image of a piece of silica with topographical asperities caused by the metal deposit on its surface (E) SEM of a clean piece of silica (not acid washed) for comparison to the silica with the deposit on the surface.

XPS data for samples after 1 month weathering revealed an unexpected issue with the current experimental design. The expected elemental composition of the plastic surface was carbon, oxygen, and a small amount of silicon from the silica sand that was used as the abrasive. However, the XPS data showed a substantial amount of chromium (12.48%) and iron (5.98%) on the surface of the plastic after weathering in 50°C conditions for 1 month (**Table 3.2**). SEM-EDS (scanning electron microscopy-energy dispersive spectroscopy) analysis was utilized to examine the degree of contamination and the physical topography of the deposit on the sample surface. SEM revealed that there was a visible delineation between where the metal had deposited on the sample and the area

where there was less deposit (**Figure 3.1**). EDS of both sides of the visible border supported that it was the metals causing the deposit as it found chromium and iron on the deposit surface, both of which were not present on the virgin sample. The source of these metals was likely the stainless-steel wells that were used in the original design. It was hypothesized that the silica particles abraded the inner sides of the well, leading to the generation of metal micro and nano-particles which formed an oxidized residue on the plastic substrate. This hypothesis was further supported by EDS of the silica (which had become an orange-ish red color over the weathering time-period) because it found substantial metal deposit on the silica itself.

From high-resolution oxygen XPS results, it was deduced that the chromium and iron were present in oxide form (**Figure 3.3)**. The oxygen peak at ~529.8 eV is indicative of both chromium (Werfel et al., 1983) and iron (McIntyre et al. 1977) oxides. This peak overlapped with the primary oxygen peak that originated from the oxidation of LDPE at ~532.0 eV (Russo et al., 1998). Due to this overlap, rather than a secondary peak formation, a broadening and shift of the original oxygen peak from the virgin sample was observed (**Figure 3.3**). The oxygen peak shift to metal oxides was more evident in the sample weathered in 50 °C conditions compared to that in room temperature, similarly the atomic percentage of chromium, iron, and oxygen were also higher in the sample weathered in 50 °C conditions (**Table 3.2**). This suggested that the higher temperature led to more rapid deposition of metal onto the plastic surface. More importantly, it was previously found that the presence of transition metals in abrasives or blades (in microtoming experiments) could lead to enhanced oxidation during abrasion and cutting (Jacobson et al., 2001). Thus, the oxidation discovered might be due to the catalytic oxidation of LDPE from the unexpected

metal deposit on the plastic surface. For this reason, in subsequent experiments, commercially available glass wells (Quark Enterprises Inc, Deerfield Township, NJ) will be utilized to replace the stainless-steel wells.

3.2.2 High Resolution Carbon XPS of Weathered LDPE

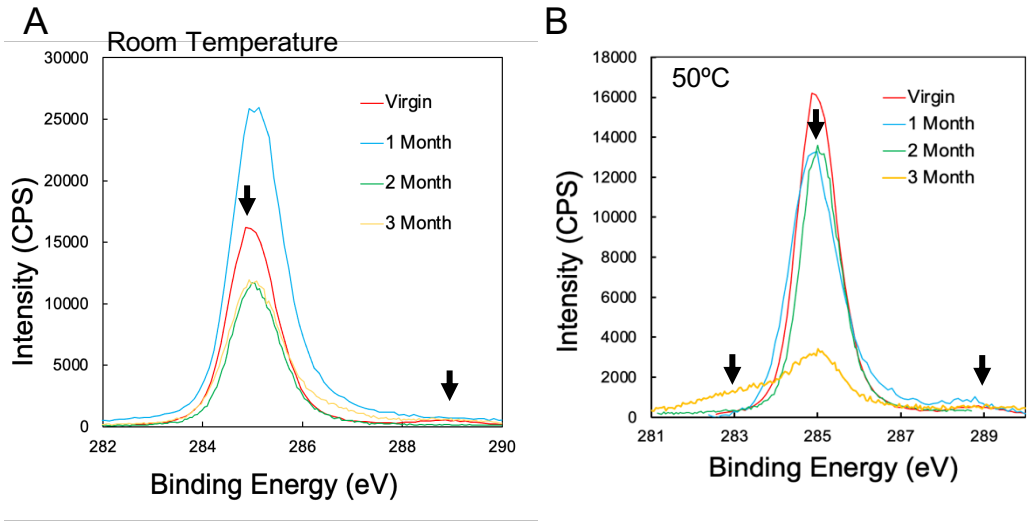

Figure 3.2. Carbon XPS result of samples weathered in (A) room temperature and (B) 50 ºC for 0 to 3 months. A small peak at (289 eV) in some of the samples indicates the presence of carbonyl group generation on the LDPE during weathering.

To help eliminate the influence of the metal oxides on the data and better examine mechanical oxidation on its own, the high-resolution carbon XPS data was analyzed. In theory this would be more indicative of mechanical oxidation compared to the oxygen peak because the metal oxides would not be represented in the carbon peak. Note that this analysis cannot exclude the impact of enhanced plastic oxidation due to the catalytic oxidation by metal deposits. The high-resolution carbon data included two notable peaks: a major peak at 285.0 eV that was present in all samples and is associated with the aliphatic carbon in LDPE (Barth et al., 1998) and a small secondary peak at approximately 289 eV

which indicates carbonyl group formation (Briggs et al., 1992). This secondary peak was observed particularly well in some weathered samples, and is potentially due to mechanical oxidation from the sediment abrasion in the system. When compared to a method blank with only water and no sand, the peak at 289 eV was eliminated (**Figure 3.4)**, implying the removal of the carbonyl group or any additional contaminants via fluid shear. Furthermore, a peak at ~283 eV was observed in the 3 month sample that was weathered in 50 °C, indicating potential carbide formation. This is unlikely given the temperature of the reaction, but silicon (Bozack, 1997), chromium (Obrosov et al., 2017), and iron (Goretzki et al. 1989) carbides all have signals near where the peak formation is. To further investigate the potential of this would require consultation with specialists in organometallics/carbides and their formation.

Overall, the degree of plastic oxidation due to sediment abrasion in this current set up in both temperatures was not obvious. It is hypothesized that mechanical oxidation under the load, type of sediment interaction, and sediment shape/surface asperity in this current setup would be too slow to be captured under current three-month experimental period. It is also hypothesized that the level of dissolved oxygen in water would be too limited to yield measurable oxidation. As the motion in this experiment simulates a typical swash zone environment (Chubarenko et al., 2020), the results also suggest that mechanical oxidation in water by regular sand would be limited; mechanical oxidation in air (e.g., surface or unsaturated soil) would most likely occur faster than that in an aquatic environment. This is further discussed below. Sharper sand with more surface asperities will also be utilized in future experiments to generate more abrasion within the system.

3.2.3 High Resolution Oxygen XPS of Weathered LDPE

Table 3.2. Atomic percentages of elements on the surface of the weathered samples. The periodic increase and decrease of the oxygen on the samples supports the hypothesis of fatigue wear within the system. The deposition of metal is also revealed by the fluctuating iron and chromium concentrations on the sample surface.

Weathering Condition	Weathering Time	Carbon (%)	Oxygen (%)	Silicon (%)	Chromium (%)	Iron (%)	Calcium (%)
Virgin	0 Month	89.43	8.12	0.90	n/a	n/a	1.55
50ºC	1 Month	49.09	30.46	2.00	12.48	5.98	n/a
	2 Month	88.26	7.09	0.00	2.84	1.81	n/a
	3 Month	62.30	27.10	9.87	0.00	0.72	n/a
Room Temperature	1 Month	92.3	7.2	0.20	0.20	0.20	n/a
	2 Month	96.54	2.89	0.39	0.10	0.07	n/a
	3 Month	77.19	19.21	0.89	1.47	n/a	n/a

In high-resolution oxygen XPS results, a major peak at 532 eV was present in all samples, which was indicative of carbonyl groups (Russo et al., 1998). Some of the carbonyl formation was likely from plastic oxidation during the hot-pressing process and is evidenced by peak presence even in the non-weathered virgin sample. It is likely that oxidation of LDPE would occur during the pressing process because the platens are heated to 180 ºC and thermal oxidation experiments of LDPE can be conducted at only 85 ºC (Kaci et al., 1999). In the samples weathered in room temperature conditions, a broadening of the primary peak at ~532 eV was observed at the end of the first month, indicating the formation of a secondary peak with a signal close to 532 eV. This shift is likely due to the deposition of the metal oxides mentioned earlier. Interestingly, the oxygen peak for the 2 month room temperature sample shifted to a higher binding energy ~ 532.8 eV (Beamson et al., 1992), indicating more carbonyl group formation over metal deposition during the second month of weathering. This peak broadening persisted until the 3rd month of

weathering, and the peak shifted again slightly towards the lower energy end, suggesting more metal deposition. This proposed transition can be verified by the atomic composition of metals over the weathering time (**Table 3.2**). The chromium and iron concentrations at 1 month and 3 months are higher than that at 2 months. Such temporal variation will be further explained later in this section. The peaks in the 50 ºC weathered samples only skewed towards the lower end of the spectrum, with the exception of a dual peak formation at 3 months, indicating that metal oxides dominated in all months. The atomic percentage of oxygen in samples weathered in 50 ºC ranged from 7.09% to 30.46%, compared to 2.89 to 19.21% for the room temperature samples. The difference between samples at the two temperatures again suggests faster deposition of metal oxide onto the plastic surface in 50 ºC conditions, which is also supported by atomic percentage results of the metals in the 50 ºC setup (**Table 3.2**).

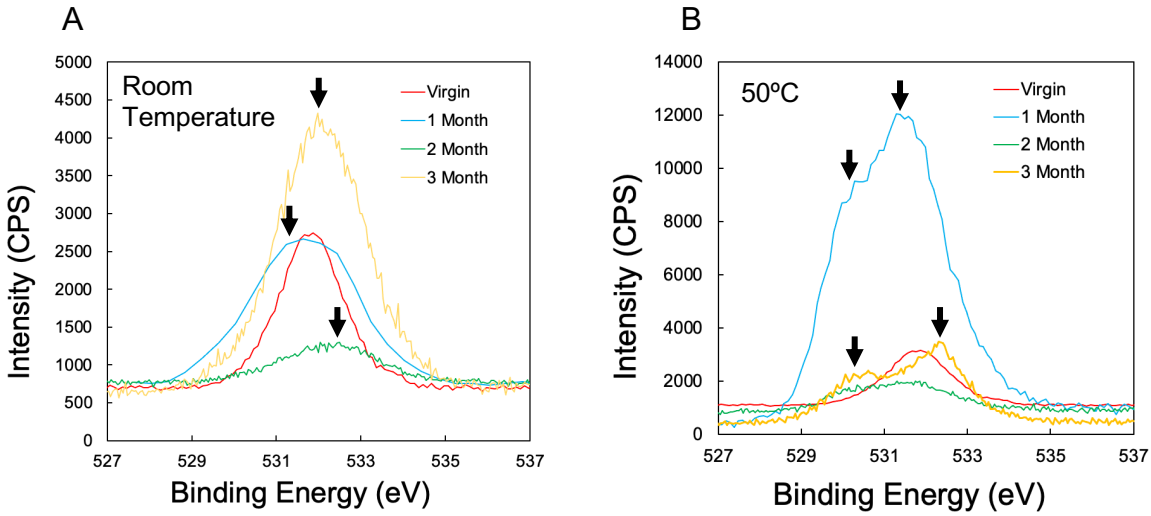

Figure 3.3. Oxygen XPS result of LDPE weathered in (A) room temperature and (B) 50 °C for 0 - 3 months. Skewing of the peak at 532 eV to lower energy of the spectrum (~529.8 eV) implies that the existence of metal oxide deposit on the surface of the sample and skewing of the peak to the higher end of the energy spectrum (~532.8 eV) implies the carbonyl group formation on the sample surface.

The dual peak formation in the 3 month sample demonstrates skewing both to the higher end of the binding energy spectrum and the lower end. The peak at the lower end is in the same position as the other metal oxide peaks, and the peak at the higher end is in a similar position as the broadening due to carbonyl formation. This data supports the hypothesis of an oxidation reaction on the plastic surface catalyzed by the deposition of metals.

Comparing the results to a control without sand (**Figure 3.4**), it was observed that the oxygen percentage actually decreased from the virgin sample implying removal of some surface contaminants by the fluid shear in the system. The peak also shifted slightly towards the higher end of the spectrum (~532.8) which is, as stated above, indicative of carbonyl formation. One possible explanation for this observation would be that with the

surface contamination removed any contribution from dust or organic contaminants on the surface would be eliminated and all that would be left is the oxygen contribution from the oxidation due to pressing. This is, however, not in agreement with the high-resolution carbon XPS data. An alternative explanation for the peak shift is that the blank samples were in the desiccator cabinet for a longer period than the other samples before they were measured, so there could be some potential trace amounts of contamination on the surface of the sample from the chemicals stored in the bottom shelf of the cabinet.

Ultimately this data confirms that, due to the metal contamination, the degree of plastic oxidation due to sediment abrasion cannot be determined through the oxygen peaks alone. The blank data, even though there is some ambiguity relating to the oxygen peak position, confirmed that the source of oxidation in the system is abrasion by sediment, metal deposition, or a combination of the two because there was substantial oxidation seen at the 1 month time point in the samples containing sand (**Table 3.2)**.

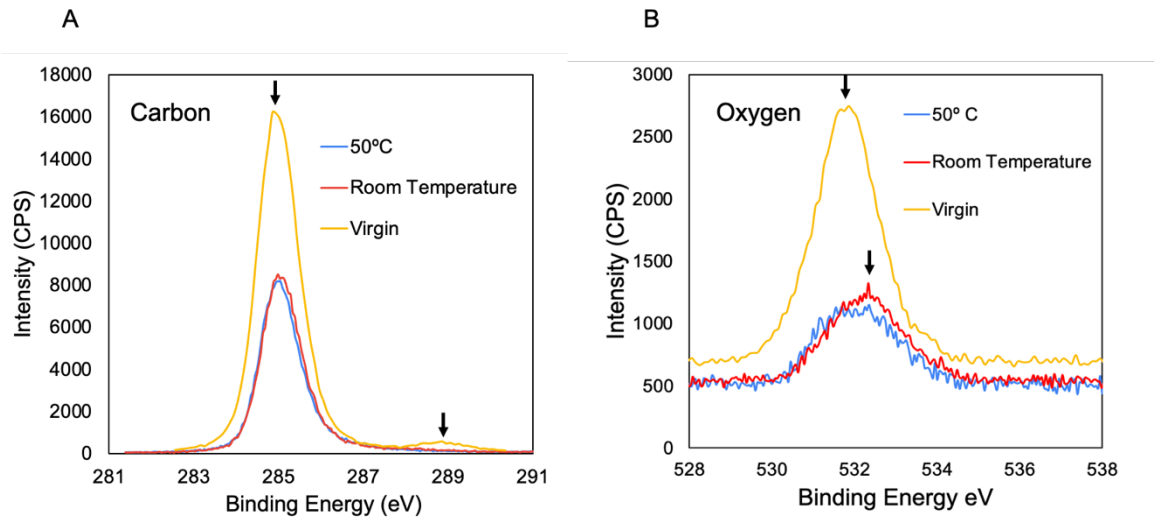

Figure 3.4. High-resolution XPS data for the control samples for (A) Carbon and (B) Oxygen which were weathered in water without sand for one month in both room temperature and 50ºC conditions. The control samples both had a lower oxygen percentage on the sample surface than the virgin sample. There was a decrease in the carbonyl peak from the virgin sample to the blank sample in the carbon data suggesting that oxidation stemming from organic contaminants or plastic pressing was potentially removed by the gentle fluid shear of the water in the device. There was also a small shift in the oxygen peak towards the higher end of the energy spectrum which could either contradict the carbon data and imply carbonyl formation, or it could be caused by sample surface contamination from the atmosphere within the desiccator cabinet.

Table 3.3. Atomic percentages for the elements found on the surface of the 1 month weathered blanks which reveal a decrease in oxygen content on the surface of the plastic after weathering in just water with no sand. This method blank confirms the source of oxidation in the system is either sand abrasion, metal deposition, or both in tandem.

Sample	Carbon (%)	Oxygen (%)	Silicon (%)	Chromium (%)	Iron (%)
Virgin	89.43	8.12	0.9	n/a	n/a
50 ºC Blank	92.49	6.12	0.77	0	0.62
Room Temperature Blank	91.2	6.79	1.5	0.15	0.36

3.2.4 Periodic fluctuation in oxidation

A periodic fluctuation in the oxygen percentage was observed on the sample surface over the three-month weathering time in 50 ºC conditions (**Table 3.2**). A similar trend was observed in samples weathered in room temperature conditions. For a cutting wear mechanism, a small piece of polymer is abraded off from plastic surface by every impact of the sediment at a localized contact point. The mechanism would then be expected to produce a gradual increase in oxygen content over time. However, the oxygen on the plastic surface increased, decreased, and increased again over three months. It is hypothesized that such periodic changes in the surface oxygen level are potentially caused by the fatigue wear mechanism, which is especially prominent under low load scenarios applied with a blunt abrasive. Given the surface asperity and shape of the sand which was used, fatigue wear is likely to be the dominant interaction.

In fatigue wear, instead of abrading off a piece of polymer material with each collision like cutting wear, sand collisions embrittle the network of the material beyond the localized contact point (Hollander et al., 1973). This embrittlement could then lead to oxidative chain scission which would slowly increase the level of oxygen on the sample surface. At a critical point of embrittlement, after continuous fatigue wear, a layer of the oxidized material would be abraded off and detach from the surface (as nanoplastics). This exodus of a large portion of the surface would then expose a fresh layer of polymer with very little oxidation. The periodic oxygen fluctuation observation, along with an illustration of the hypothesized fatigue wear weathering that coincides with it, is illustrated in **Figure 3.5**. This fluctuation in oxygen was accompanied by metal concentration fluctuation in the 50 ºC sample (**Table 3.2**) where metal deposition was high in the first month, decreased in the second month, and increased again in the third month. This suggests that the deposited

metal layer was fatigued until a certain time after which it then detached from the sample surface. According to this result, the time for a fatigue wear cycle to occur is on the order of 1-2 months. To verify this hypothesis, in future experiments samples will be collected 2 times per month.

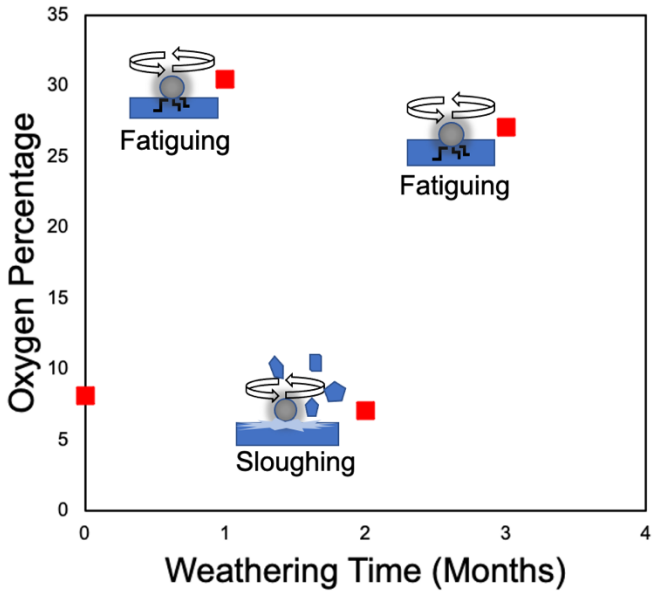

Figure 3.5. Oxygen percentages of LDPE weathered at room temperature decreased from 1 to 2 months, then increased again at month 3. Such fluctuating oxygen level is hypothesized to reflect a fatigue wear behavior transition. The fatigue wear mechanism is also illustrated near each data point to depict what is hypothesized to be happening in the system at which time point.

3.2.5 Oxidation in Water v.s. Air

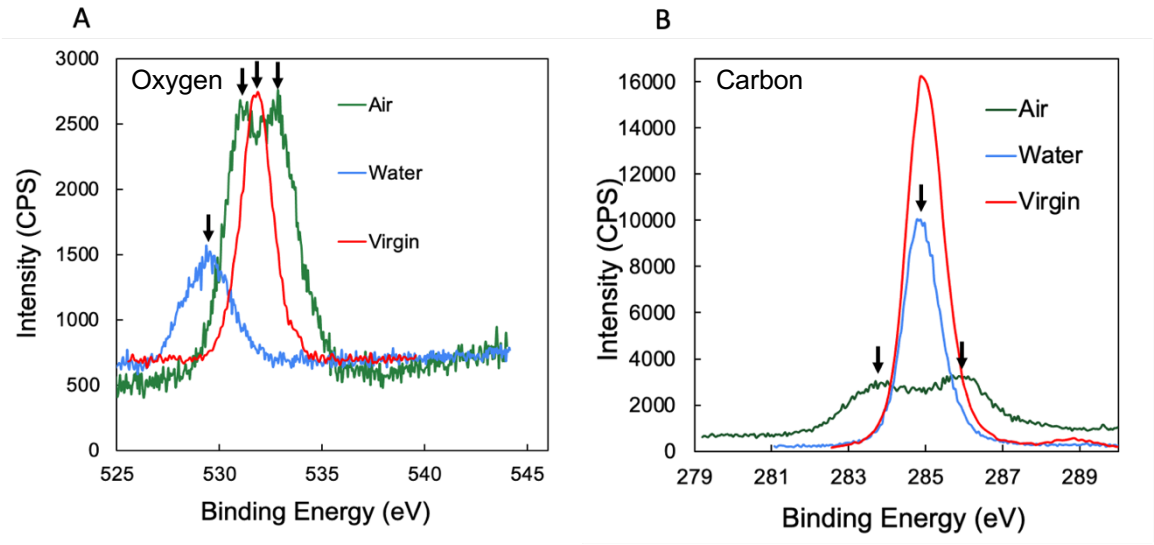

Figure 3.6. (A) Oxygen and (B) Carbon high resolution XPS data for samples weathered in air and water with sand abrasion for 5 months under 50 ºC. The water LDPE sample was covered in 400 mg of silica sand and 4 mL of ultrapure water; the air sample was just covered in 400 mg of silica sand without water. The results demonstrate that increased oxygen in air compared to water led to difference in sample surface chemistry.

To demonstrate the effect of the atmospheric level of oxygen on plastic oxidation, weathering experiments in air rather than water were also performed. After five months of abrasive weathering in 50 ºC the sample weathered in air, with a higher ambient oxygen concentration, showed a larger deviation from the virgin peak and a dual peak formation in the both the carbon and oxygen high-resolution XPS data. The two peaks formed in the carbon data at ~284.5 eV (Beamson et al., 1992) and ~286.1 eV (Dilks et al., 1981) are both indicative of carbonyl formation, suggesting a significant degree of oxidation of plastic in the air conditions due to abrasion. In comparison, the water weathered sample had an identical primary peak to the virgin sample at 285 eV, which is representative of the aliphatic carbon in LDPE. The two peaks formed in the air sample for the oxygen data at ~531.3 eV and ~532.8 eV (Beamson et al. 1992) were also indicative of carbonyl

formation, supporting the finding from carbon peak. In comparison, the major oxygen peak in the water sample shifted from 532 eV in the virgin sample to ~529.8 eV which indicates both iron and chromium oxides deposits, after five months of weathering. The presence of iron and chromium oxides is also supported by the atomic percentages listed below in **Table 3.4** Interestingly, severe metal deposition was not observed in the air sample, suggesting that metal leaching from the stainless-steel well was somehow assisted by the presence of water. The air sample was originally designed as a control to eliminate the effect of fluid shear in the setup, so there was not an air blank (no sand or water) produced by this round of experiments. Given this interesting result, the effect of ambient oxygen concentration will be investigated in future experiments. It will also be ensured that said experiments will have a blank where the plastic is just kept in atmospheric conditions for the desired weathering times at both temperatures.

Table 3.4. Atomic percentages of the different elements present on the surface of the samples weathered for five months at 50 ºC in both air and water. These percentages reveal a significantly larger amount of oxidation on the surface of the sample weathered in air, this is hypothesized to be due to more abundant oxygen.

Sample	Carbon (%)	Oxygen (%)	Silicon (%)	Chromium (%)	Iron (%)
Virgin	89.43	8.12	0.9	n/a	n/a
Air	69.82	24.08	3.14	2.79	0.18
Water	84.27	7.23	0.28	1.94	1.01

In summary, XPS provided valuable insight into the surface chemistry of abrasion in water and air, under the two weathering temperatures. XPS data informed that mechanical oxidation in water under the current sediment load, shape, and surface asperity

cannot yield a significant level of oxidation that is measurable by XPS. Such oxidation was observed to be higher in air, likely due to higher concentration of oxygen. These results suggest more oxidation would occur in terrestrial environment compared to an aquatic environment. Periodic fluctuations in amounts of oxygen and metal on the sample surface suggest a fatigue wear mechanism instead of cutting. The unexpected contamination from stainless steel interfered with the hypothesis testing thus, glass wells will replace the use of stainless-steel in future experiments. Note that the abrasion from glass wells would also be inevitable (glass that is abrasion resistant to silica is very difficult to fabricate), but the composition of glass will eliminate the possibility of enhanced oxidation by transition metals.

3.3 Nano-plastic Quantification and Characterization

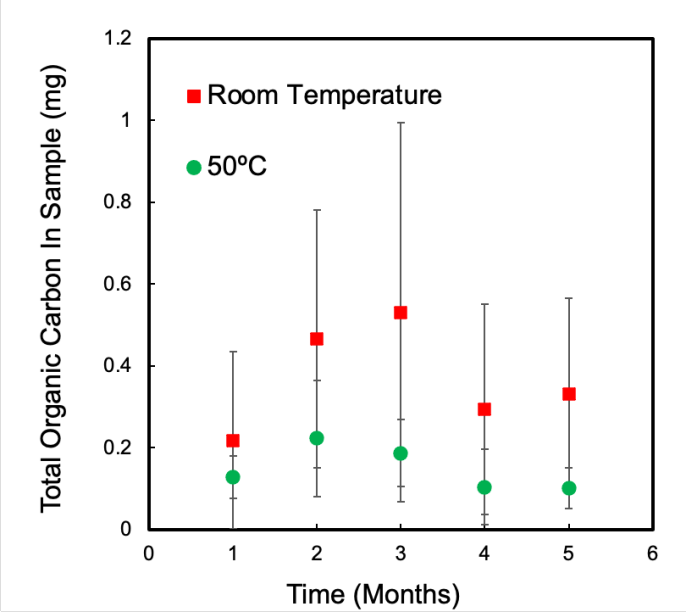

Figure 3.7. The total organic carbon mass in each sample over the five months. Due to evaporation in the fluid cell, the total mass of carbon leached was calculated by multiplying TOC with final volume of fluid. Constant evaporation in both setups was also potentially causing the decrease in TOC in the samples for the later month samples. The decrease may happen sooner in the 50 ºC samples because the evaporation is more rapid in that setup.

To investigate the quantity of micro- and nano- plastics produced during weathering, total organic carbon (TOC) was measured to detect the dissolved and particulate carbon in the suspension at all sizes as a proxy measurement for micro and nano-plastics. Nanoparticle tracking analysis (NTA) was also utilized to directly measure particles with sizes ranging from 30 nm – 1 μm. An increase in TOC and particle concentration was hypothesized in the fluid sample over the weathering time due to plastic particles being abraded off from the surface of the bulk plastic.

Due to evaporation of the fluid in each cell, which was particularly fast at the higher temperature, a total mass of carbon leached was calculated by multiplying TOC by the final volume of the fluid sample. In contrast to the expected result, for samples in both temperatures, the mass of carbon slightly increased within the first few months and then actually decreased (**Figure 3.7.**). The dissolved carbon for samples weathered in 50 ºC had a large error bar and was overall slightly lower than the samples weathered in room temperature. This comparison is inconclusive due to the large error bar in the data. As previously stated, there was significant water evaporation in both temperatures, leading to residue formation on the sides of each well at the end of weathering. As ultrapure water was used for the experiments, it is hypothesized that the residue likely consists of plastic particles aggregating and depositing on the inner wall of the well during evaporation. Refilling of water was performed twice a week in the 50 ºC setup and a few times a month in the room temperature setup in an attempt to keep a constant sediment motion and water level. During the refilling and after the samples were removed the residue persisted even with repeated rinsing implying that once aggregated to the side of the well, any plastics in the residue would remain stuck there. The 50 ºC experimental setup had a more rapid

evaporation than the room temperature one, which is why it is hypothesized the decreases in concentration started sooner in that setup than in the room temperature setup.

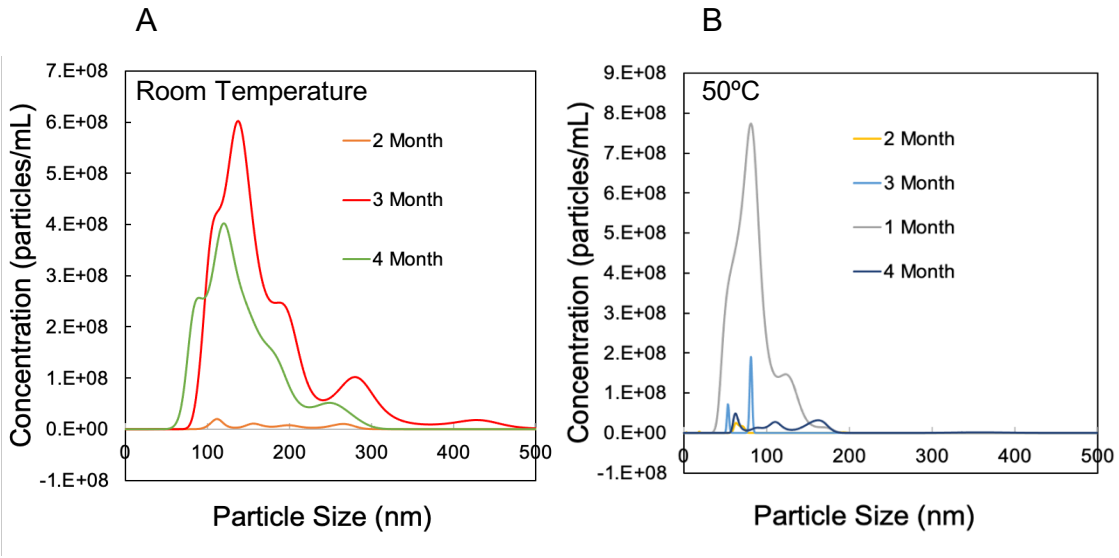

Figure 3.8. Number concentration of particles measured by Nanoparticle Tracking Analysis (NTA) from the sample weathered at room temperature (A) and 50ºC (B). The 1 month weathered sample in room temperature conditions was not included due to the fact sample was under the detection limit for NTA. A combination of evaporation and centrifugal force induced aggregation may cause the decrease in particle concentration and increase in polydispersity over weathering time.

In tandem with the proxy TOC measurements made, direct analysis of the nano particles generated during abrasive weathering was performed using NTA. Measured concentrations were from 0.5×10^8 - 8×10^8 particles/mL and the particle size ranged from about 50 – 500 nm which suggests the generation of primarily nano-sized particles (i.e., nano-plastics). The NTA data in this experiment was, again, expected to increase over the course of the weathering period. It was also suspected that, since the oxidation rate was expected to increase at a higher temperature, the 50 ºC samples would have a larger nano-plastic concentration than the room temperature samples. This is because as plastic is oxidized it becomes embrittled and would hypothetically abrade faster. This was supported

when the 1 month room temperature sample was so dilute that it was under detection limit for NTA and the one month sample for 50 ºC had a concentration of approximately 8×10^8 particles/mL.

The following months data, however, did not agree with expectations. For room temperature samples, the concentration increased by 6-fold from 2-3 months and the sample also became much more polydisperse. This polydispersity is likely due to particle aggregation or the generation of larger particles over time. However, the particle concentration decreased to about 4×10^8 particles/mL in month 4. It was also observed that the 3 month sample was more polydisperse compared to 4 month sample, suggesting a larger fraction of particles either aggregated into a larger size that is over the detection limit of the NTA, or particles were aggregating to the sides of the well and thus did not remain in suspension. For the 50 ºC samples, the particle concentration was 8×10^8 particles/mL after 1 month, but this drastically declined at 2-4 months. This is, however, in agreement with the trend in TOC data, supporting the hypothesis that aggregated particles were attached and lost to the inner wall of the reactor. In addition to evaporation, the rotational motion of the fluid could also create a minor shear gradient and centrifugal force that facilitates aggregation and particles moving to the wall of the well. To mitigate the effect of aggregation on future data both number and volume concentrations will be analyzed for the samples generated in future experiments.

In summary nanoparticle analysis did not reveal the expected trend, but rather indicated an issue with the experimental design that will be addressed later within this paper. The rapid evaporation in both setups is hypothesized to have caused the decrease in both particle number and TOC concentrations in the fluid samples over the course of the

weathering experiment. Number concentration measurements from NTA were even more confounding than the TOC data, which is hypothesized to be due to further aggregation of the particles to one another. This further aggregation would also generate the increase in polydispersity that was seen.

4. CONCLUSION

4.1 Significance of Current Findings

There were significant setbacks of the preliminary design of fluid cell and experiment, leading to inconclusiveness of the results. Ultimately, due to the metal oxide deposit on the surface of the sample, it is impossible to make any definitive conclusions about whether mechanical oxidation is happening in the apparatus. However, significant findings can be concluded from these preliminary results that will inform future research. Analysis of the high-resolution carbon and oxygen data indicates the formation of carbonyl groups as a result of abrasive wear by sand. We also found that oxidation in this apparatus occurs much more rapidly in air compared to water due to the abundance of oxygen. With further experiments, that eliminate the impact of metal oxides, it could be inferred that mechano- oxidation would occur much more rapidly in soil environments than in aquatic environments. This could be applied to inform the fate and lifetime of plastic waste that is currently residing in agricultural soil and landfill soil settings. The preliminary results also suggest the utility of a sharper sand, where the rate of nano-plastic formation can then be measured in reasonable time frame due to more rapid nano-plastic generation from a more cutting wear-oriented mechanism. Such results would imply the quantity of nano-plastics

that could be released in future years from bulk plastics that are intentionally (e.g., mulch film) and unintentionally (e.g., mismanaged plastic waste) released into the natural environment. Finally, the newly hypothesized fatigue wear mechanism informs the role of sediment sharpness and surface asperity in the wear mechanism, and the subsequent rate of plastic oxidation and characteristics of nano-plastic release.

4.2 Future Work and Improvements

The presence of chromium and iron oxides compromised the high-resolution oxygen data from the XPS analyses and could have potentially catalyzed additional oxidation on the surface of the polymer itself. The stainless-steel wells have been replaced with tempered glass that is combusted to remove any residual organics.

Rapid evaporation of water from wells impacted TOC and nano-plastic quantification, especially in the 50 °C setup. The potential leaky joints in the design have been tested and identified: there are two joints near the top of the fluid cell, one is between the acrylic lid and the top piece of Delrin, and the second is between the top of the well and the top piece of Delrin. A preliminary experiment where these two joints were sealed with caulk showed that the water level was, for the most part, was maintained over two weeks under 50 °C, whereas all 4 mL of ultrapure water would have evaporated within a week in the original design. These leaks will be addressed by adding a high-temperature silicon sheet between the acrylic lid and the top piece of Delrin to serve as a gasket and generate a better seal. The joint between the well and the top plate will be amended with the addition of food grade silicon O-rings that will be clamped between the well and the Delrin. The high temperature silicon will be utilized because it is known to be non-reactive

and not off-gas at higher temperatures, as off-gassing could influence sensitive XPS measurements.

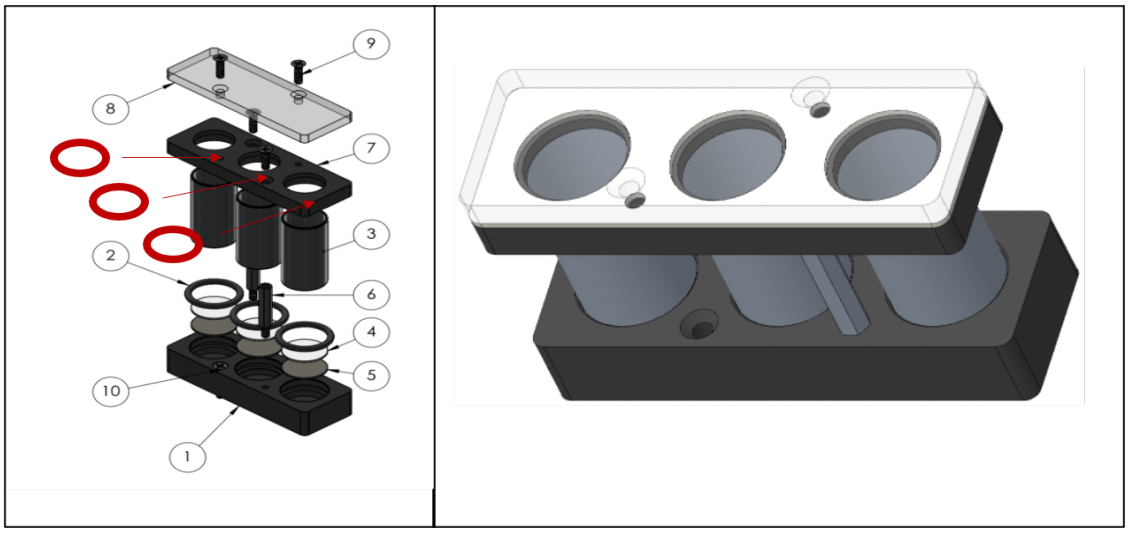

Figure 4.1. Amendments made to the initial experimental setup to mitigate evaporation including the placement of additional O-rings (A) and a gasket-like silicon interfacial plate to generate a tighter seal between the top two pieces shown in white (B).

Preliminary findings on the significant effect of oxygen availability inform future experiments with an emphasis on the medium in which the weathering is taking place, in addition to abrading material. The additional experiments in air will be more representative of soil environments. Furthermore, to investigate cutting wear versus the current hypothesized fatigue wear mechanism, the abrading sediment will be substituted with crushed glass as a sharper abrasive to potentially generate cutting wear within the system. Lastly, more frequent sampling will test the hypothesis of periodic fluctuation of oxygen due to fatigue wear.

With clear room for improvement, this thesis summarizes design and preliminary testing of a device that successfully simulates an abrasive-wear weathering environment for bulk plastic and produces both fluid and substrate plastic samples that have the potential

to be analyzed for both oxidation and nano-plastic quantification. A successful workflow of sample analyses has also been established, and precautions were formulated for the second round of experiments. In addition to the simulated environment, this device has great potential due to its high-throughput nature and its ability to accommodate multiple different weathering environments. It also allows for a wide range of testing conditions given how easily experimental conditions can be altered by changing the substrate, abrasive material, or weathering medium. It is also readily replicable because of its use of basic laboratory equipment as the main dynamic component. The future work relating to this device will help to deconvolute oxygen sources in the system and improve accuracy of micro and nano particle analysis. Given the potential external source of oxidation with the metal oxide deposit and the inconclusive micro/nanoparticle data caused by evaporation in the device, it was not possible to generate a reliable correlation between work and oxidation/particle production. However, given these added improvements, this experimental setup shows great promise in its ability to generate an accurate correlation between work input into a polymer surface and the resulting oxidation and nano-plastic production.

References

(1)

Barth, G.; Linder, R.; Bryson, C. Advances in Charge Neutralization for XPS Measurements of Nonconducting Materials. Surface and interface analysis 1988, 11 (6-7), 307–311. https://doi.org/10.1002/sia.740110607.

(2)

Beamson, G.; Briggs, D. High Resolution Monochromated X-Ray Photoelectron Spectroscopy of Organic Polymers: A Comparison Between Solid State Data for Organic Polymers and Gas Phase Data for Small Molecules. Molecular physics 1992, 76 (4), 919–936. https://doi.org/10.1080/00268979200101761.

(3)

Briggs, D.; Beamson, G. XPS Studies of the Oxygen 1s and 2s Levels in a Wide Range of Functional Polymers. Analytical chemistry (Washington) 1993, 65 (11), 1517–1523. https://doi.org/10.1021/ac00059a006.

(4)

Brundle, C. R.; Crist, B. V. X-Ray Photoelectron Spectroscopy: A Perspective on Quantitation Accuracy for Composition Analysis of Homogeneous Materials. Journal of vacuum science & technology. A, Vacuum, surfaces, and films 2020, 38 (4), 41001. https://doi.org/10.1116/1.5143897.

(5)

Bozack, M. J. Surface Studies on SiC as Related to Contacts. physica status solidi (b) 1997, 202 (1), 549–580. https://doi.org/10.1002/1521-3951(199707)202:1<549::AID-PSSB549>3.0.CO;2-6.

(6)

Chamas, A.; Moon, H.; Zheng, J.; Qiu, Y.; Tabassum, T.; Jang, J. H.; Abu-Omar, M.; Scott, S. L.; Suh, S. Degradation Rates of Plastics in the Environment. ACS sustainable chemistry & engineering 2020, 8 (9), 3494–3511. https://doi.org/10.1021/acssuschemeng.9b06635.

(7)

Chubarenko, I.; Efimova; Bagaeva; Bagaev; Isachenko. On Mechanical Fragmentation of Single-Use Plastics in the Sea Swash Zone with Different Types of Bottom Sediments: Insights from Laboratory Experiments. Marine pollution bulletin. 2020, 150. https://doi.org/10.1016/j.marpolbul.2019.110726.

(8)

Costa, L.; Luda, M. .; Trossarelli, L. Ultra-High Molecular Weight Polyethylene: I. Mechano-Oxidative Degradation. Polymer degradation and stability 1997, 55 (3), 329–338. https://doi.org/10.1016/S0141-3910(96)00170-X.

(9)

Dilks, A.; Clark, D. T. ESCA Studies of Natural Weathering Phenomena at Selected Polymer Surfaces. Journal of polymer science. Polymer chemistry edition 1981, 19 (11), 2847–2860. https://doi.org/10.1002/pol.1981.170191118.

(10)

Ekvall, M. T.; Gimskog, I.; Hua, J.; Kelpsiene, E.; Lundqvist, M.; Cedervall, T. Size Fractionation of High-Density Polyethylene Breakdown Nanoplastics Reveals Different Toxic Response in Daphnia Magna. Scientific reports 2022, 12 (1), 3109–3109. https://doi.org/10.1038/s41598-022-06991-1.

(11)

Enfrin, M.; Lee, J.; Gibert, Y.; Basheer, F.; Kong, L.; Dumée, L. F. Release of Hazardous Nanoplastic Contaminants Due to Microplastics Fragmentation Under Shear Stress Forces. Journal of hazardous materials. 2020, 384. https://doi.org/10.1016/j.jhazmat.2019.121393

(12)

Fanconi, B. .; DeVries, K. .; Smith, R. . Free Radicals and New End Groups Resulting from Chain Scission: 2. Mechanical Degradation of Polyethylene. Polymer (Guilford) 1982, 23 (7), 1027–1033. https://doi.org/10.1016/0032-3861(82)90403-7.

(13)

Gao, J.; Luedtke, W. D.; Gourdon, D.; Ruths, M.; Israelachvili, J. N.; Landman, U. Frictional Forces and Amontons' Law: From the Molecular to the Macroscopic Scale. The journal of physical chemistry. B 2004, 108 (11), 3410–3425. https://doi.org/10.1021/jp0363621.

(14)

Giesse, R.; De Paoli, M.-A. Surface and Bulk Oxidation of Low-Density Polyethylene Under UV-Irradiation. Polymer degradation and stability 1988, 21 (2), 181–187. https://doi.org/10.1016/0141-3910(88)90048-1.

(15)

Geyer, R.; Jambeck, J. R.; Law, K. L. Production, Use, and Fate of All Plastics Ever Made. Science advances 2017, 3 (7), e1700782–e1700782. https://doi.org/10.1126/sciadv.1700782.

(16)

Goretzki, H.; Rosenstiel, P. v.; Mandziej, S. Small Area MXPS- and TEM-Measurements on Temper-Embrittled 12% Cr Steel. Fresenius' Zeitschrift für analytische Chemie 1989, 333 (4-5), 451–452. https://doi.org/10.1007/BF00572350.

(17)

Hollander, A.E.; Lancaster, J. . An Application of Topographical Analysis to the Wear of Polymers. Wear 1973, 25 (2), 155–170. https://doi.org/10.1016/0043-1648(73)90068-9.

(18)

Hsu, Y.-C.; Weir, M. P.; Truss, R. W.; Garvey, C. J.; Nicholson, T. M.; Halley, P. J. A Fundamental Study on Photo-Oxidative Degradation of Linear Low Density Polyethylene Films at Embrittlement. Polymer (Guilford) 2012, 53 (12), 2385–2393. https://doi.org/10.1016/j.polymer.2012.03.044.

(19)

Jacobson, K.; Costa, L.; Bracco, P.; Augustsson, N.; Stenberg, B. Effects of Microtoming on Oxidation of Ultra High Molecular Weight Polyethylene (UHMWPE). Polymer degradation and stability 2001, 73 (1), 141–150. https://doi.org/10.1016/S0141-3910(01)00080-5.

(20)

Jahnke, A.; Arp, H. P. H.; Escher, B. I.; Gewert, B.; Gorokhova, E.; Kühnel, D.; Ogonowski, M.; Potthoff, A.; Rummel, C.; Schmitt-Jansen, M.; Toorman, E.; MacLeod, M. Reducing Uncertainty and Confronting Ignorance About the Possible Impacts of Weathering Plastic in the Marine Environment. Environmental Science and Technology Letters 2017, 4 (3), 85–90. https://doi.org/10.1021/acs.estlett.7b00008.

(21)

Kaci, M.; Cimmino, S.; Di Lorenzo, M. L.; Silvestre, C.; Sadoun, T. EFFECT OF THE THERMO-OXIDATION AND NATURAL WEATHER ON THE STRUCTURE, MORPHOLOGY, AND PROPERTIES OF UNSTABILIZED AND HALS-STABILIZED LDPE FILMS. Journal of macromolecular science. Part A, Pure and applied chemistry 1999, 36 (2), 253–274. https://doi.org/10.1080/10601325.1999.10504907.

(22)

Kalogerakis, N.; Karkanorachaki, K.; Kalogerakis, G. C.; Triantafyllidi, E. I.; Gotsis, A. D.; Partsinevelos, P.; Fava, F. Microplastics Generation: Onset of Fragmentation of Polyethylene Films in Marine Environment Mesocosms. Frontiers in Marine Science 2017, 4. https://doi.org/10.3389/fmars.2017.00084.

(23)

Kurtz, S. M.; Rimnac, C. M.; Hozack, W. J.; Turner, J.; Marcolongo, M.; Goldberg, V. M.; Kraay, M. J.; Edidin, A. A. In Vivo Degradation of Polyethylene Liners After Gamma Sterilization in Air. Journal of bone and joint surgery. American volume 2005, 87 (4), 815–823. https://doi.org/10.2106/JBJS.D.02111.

(24)

Lan, T.; Wang, T.; Cao, F.; Yu, C.; Chu, Q.; Wang, F. A Comparative Study on the Adsorption Behavior of Pesticides by Pristine and Aged Microplastics from Agricultural Polyethylene Soil Films. Ecotoxicology and environmental safety 2021, 209, 111781. https://doi.org/10.1016/j.ecoenv.2020.111781.

(25)

McIntyre, N. S.; Zetaruk, D. G. X-Ray Photoelectron Spectroscopic Studies of Iron Oxides. Analytical chemistry (Washington) 1977, 49 (11), 1521–1529. https://doi.org/10.1021/ac50019a016.

(26)

Obrosov, A.; Gulyaev, R.; Zak, A.; Ratzke, M.; Naveed, M.; Dudzinski, W.; Weiß, S. Chemical and Morphological Characterization of Magnetron Sputtered at Different Bias Voltages Cr-Al-C Coatings. Materials 2017, 10 (2), 156. https://doi.org/10.3390/ma10020156.

(27)

Potyrailo, R.; Rajan, K.; Stoewe, K.; Takeuchi, I.; Chisholm, B.; Lam, H. Combinatorial and High-Throughput Screening of Materials Libraries: Review of State of the Art. ACS combinatorial science 2011, 13 (6), 579–633. https://doi.org/10.1021/co200007w.

(28)

Russo, M. V.; Polzonetti, G.; Furlani, A.; Bearzotti, A.; Fratoddi, I.; Altamura, P. X-Ray Photoelectron Spectroscopy and Scanning Electron Microscopy Characterization of Novel Poly(monosubstituted) Acetylenes Containing Doping Species. Journal of vacuum science & technology. A, Vacuum, surfaces, and films 1998, 16 (1), 35–44. https://doi.org/10.1116/1.581006.

(29)

Smith, M.; Love, D. C.; Rochman, C. M.; Neff, R. A. Microplastics in Seafood and the Implications for Human Health. Current environmental health reports 2018, 5 (3), 375–386. https://doi.org/10.1007/s40572-018-0206-z.

(30)

Sohma, J. Mechanochemistry of Polymers. Progress in polymer science 1989, 14 (4), 451–596. https://doi.org/10.1016/0079-6700(89)90004-X.

(31)

Suresh, B.; Maruthamuthu, S.; Kannan, M.; Chandramohan, A. Mechanical and Surface Properties of Low-Density Polyethylene Film Modified by Photo-Oxidation. Polymer journal 2011, 43 (4), 398–406. https://doi.org/10.1038/pj.2010.147.

(32)

Tribedi, P.; Dey, S. Pre-Oxidation of Low-Density Polyethylene (LDPE) by Ultraviolet Light (UV) Promotes Enhanced Degradation of LDPE in Soil. Environmental monitoring and assessment 2017, 189 (12), 1–8. https://doi.org/10.1007/s10661-017-6351-2.

(33)

Wahl, A.; Le Juge, C.; Davranche, M.; El Hadri, H.; Grassl, B.; Reynaud, S.; Gigault, J. Nanoplastic Occurrence in a Soil Amended with Plastic Debris. Chemosphere (Oxford) 2021, 262, 127784–127784. https://doi.org/10.1016/j.chemosphere.2020.127784.

(34)

Werfel, F.; Brümmer, O. Corundum Structure Oxides Studied by XPS. Physica scripta 1983, 28 (1), 92–96. https://doi.org/10.1088/0031-8949/28/1/013.

(35)

Xu, M.; Halimu, G.; Zhang, Q.; Song, Y.; Fu, X.; Li, Y.; Li, Y.; Zhang, H. Internalization and Toxicity: A Preliminary Study of Effects of Nanoplastic Particles on Human Lung Epithelial Cell. The Science of the total environment 2019, 694, 133794. https://doi.org/10.1016/j.scitotenv.2019.133794.

(36)

Yan, Z.; Liu, Y.; Zhang, T.; Zhang, F.; Ren, H.; Zhang, Y. Analysis of Microplastics in Human Feces Reveals a Correlation Between Fecal Microplastics and Inflammatory Bowel Disease Status. Environmental science & technology 2022, 56 (1), 414–421. https://doi.org/10.1021/acs.est.1c03924.

(37)

Yang, J. Q.; Nepf, H. M. Impact of Vegetation on Bed Load Transport Rate and Bedform Characteristics. *Water resources research* **2019**, *55* (7), 6109–6124. https://doi.org/10.1029/2018WR024404.